

Numerical simulation and optimization of the in-situ heating and cracking process of oil shale

Tengfei Sun, Hao Liu*, Yang Zhang*, Baokang Wu, Zhilei Wang, Yacong Fan, Yongan Li, Yongliang Han, Ziyang Liu

College of Mechanical and Electrical Engineering, Beijing University of Chemical Technology, Beijing 100029, China

Received 15 March 2023, accepted 14 July 2023, available online 10 September 2023

Abstract. *In this paper, the temperature field variation and cumulative oil production rate over time with fracture number, fracture width and gas injection flow rate were investigated using Fluent software. A mathematical model of heat transfer within oil shale and a three-dimensional mathematical model of its in situ heating and fracturing were established. The simulation results showed that Model II had the highest oil shale heating rate at different fracture numbers, being 26.32% higher than that of Model I. When exploring fracture width, Model I completed all fractures in the oil shale region in 190 days. Model IV was 15 days slower than Model I with the heating rate being 7.89% lower, while Model V was 10 days faster than Model I with the heating rate being 5.26% higher. Increasing the fracture width of the oil shale region appropriately could help to increase the oil shale in-situ heating and fracturing rate. Considering gas injection flow rate, the higher the gas flow rate, the faster the increase of the oil shale area temperature and the shorter the time to reach the 10-day peak oil production rate. The peak was also larger and the fracturing of the oil shale area took place more quickly.*

Keywords: *Chinese oil shale, temperature field, heating time, cumulative oil production rate, in-situ heating cracking.*

1. Introduction

Shale oil is a very abundant unconventional resource, and according to a new evaluation of oil and gas resources in China, the country ranks fourth in the world in terms of shale oil and gas reserves [1–4]. Shale oil in China is mainly distributed in 1–4 resources-rich northern regions, while the southern regions are relatively poor. Shale oil is mostly found in Jilin and Shaanxi provinces [5–7].

* Corresponding authors: e-mails 2002500011@mail.buct.edu.cn; 15103380300@163.com

Currently, the principal method of shale oil extraction in China is through surface retorting technology, which, however, is inefficient and causes serious pollution to the environment. This method is only suitable to be used in shale deposits that are thick and shallow [8]. As a result, in-situ heating and cracking technology for shale oil is receiving increasing attention from scholars and experts. This technology for shale oil involves heating the shale rock underground to crack it, after which the shale oil produced is transported to the surface through production wells [9]. At present, there are four main methods of in-situ heating and cracking technology for shale oil, including combustion heating, conduction heating, convection heating and radiation heating [10–11]. Combustion heating involves the In-situ Combustion technology developed by the United States Bureau of Mines [12]. Conduction heating comprises Shell's In-situ Conversion Process technology (ICP) and IEP's Gas Field Chromatography technology (GFC) [13]. Convection heating includes Chevron's Controlled Freeze Zone Rapid Unloading Single-Stage Hydrocracking technology (CRUSH) and Jilin University's Innovative Integrated Sorption-enhanced Vacuum Thermal Process technology (IIST-VTCP) [14]. Radiation heating incorporates LLNL's RF technology and Raytheon's Radio-Frequency/Critical Fluids technology (RF/CF) [15]. The above in-situ heating and cracking technologies for shale oil effectively avoid air and water pollution and reduce damage to land resources. The combustion heating technology has broad application prospects for the in-situ exploitation of shale oil resources [16–18].

This article discusses the in-situ heating and cracking process of oil shale, which uses a spiral heater to generate high-temperature air and heat the shale in the area [19]. By now, scholars both domestically and abroad have conducted numerical simulations of the in-situ heating and cracking process of oil shale. Kang et al. [20] studied the temperature field variation and small-scale oil and gas production during the in-situ electric heating of oil shale. Yang et al. [21] conducted numerical simulations of the in-situ heating and cracking process of oil shale and found convective heating to be a more optimal mining technology. Jiang et al. [22] used high-temperature nitrogen gas to heat the horizontal well section of oil shale, established a mathematical model, and conducted two-dimensional simulations, finding that the alternating heating of the heating well and the production well can afford higher energy utilization efficiency. Li et al. [23] researched the changes in the porosity and permeability of oil shale with temperature field during its in-situ heating and cracking. Xue and Liu [24] developed a thermal conduction mathematical model and conducted numerical simulations of the temperature field, finding that the entire system consumes a large amount of energy during the mining process, and the heat transfer in the entire oil shale layer is slow. Jiang et al. [25] performed numerical simulations of the in-situ heating and cracking process using fracturing and nitrogen injection technology, and compared the process with electric heating, discovering that the convective fracturing and

nitrogen injection technology were more effective. Wang et al. [26] studied the effects of fracture size and well group position on the heating effect during the in-situ heating and cracking process of oil shale. Zheng et al. [27] analyzed the thermal efficiency of oil shale in-situ heating and cracking using the CMG-STARS software. Ma et al. [1] performed numerical simulations of the temperature field during the in-situ heating and cracking of oil shale using Fluent software, and found that the higher the gas injection rate and the higher the number of injection wells, the better the heating effect.

Today, the main issue with numerical simulation and optimization of the in-situ oil shale heating and cracking process is that most scholars have only compared the effects of heating technique, gas temperature and heating rate on the oil shale heating process. Some investigators have also explored the effect of injecting high-temperature gas from the surface on the in-situ oil shale heating and cracking. It has been found that there is a heat loss during the injection of high-temperature air from the surface to the wellbore, which results in energy waste. Also, a few researchers have investigated the two-dimensional in-situ heating and cracking process of oil shale, but the accuracy and reference value of the process have been found to be relatively poor compared to the three-dimensional in-situ cracking of oil shale. This paper differs from the aforementioned scholars' studies mainly in that it proposes different three-dimensional oil shale models with different fracture numbers and fracture widths, using a downhole spiral heater to heat and generate high-temperature air for the in-situ heating and cracking of three-dimensional oil shale. The temperature field changes during the in-situ heating and cracking of three-dimensional oil shale were analyzed, and the effects of fracture number, fracture width and gas injection rate on the process were investigated to determine the optimal heating scheme. This provides a plan for the later field experiments on the in-situ heating and cracking of oil shale.

2. Principle of in-situ heating and cracking of oil shale

Figure 1 shows a schematic diagram of the in-situ heating and cracking of oil shale. In this study, a downhole spiral baffle heater is used to heat low-temperature air input from the surface into high-temperature air underground to heat the oil shale area. At the same time, a barrier is placed at the intersection of oil shale and the underlying rock in the heating well to prevent the heated high-temperature air from flowing into the production well. The process of heating oil shale with high-temperature air mainly involves the following steps: drilling the production well and the heating well using a drilling rig in the early stage, followed by casing and cementing. Then conventional fracturing is carried out. The horizontal fractures generated by fracturing oil shale make the production well and the heating well interconnected [28, 29]. After oil shale is fractured, the heating system is installed and air is heated. The high-

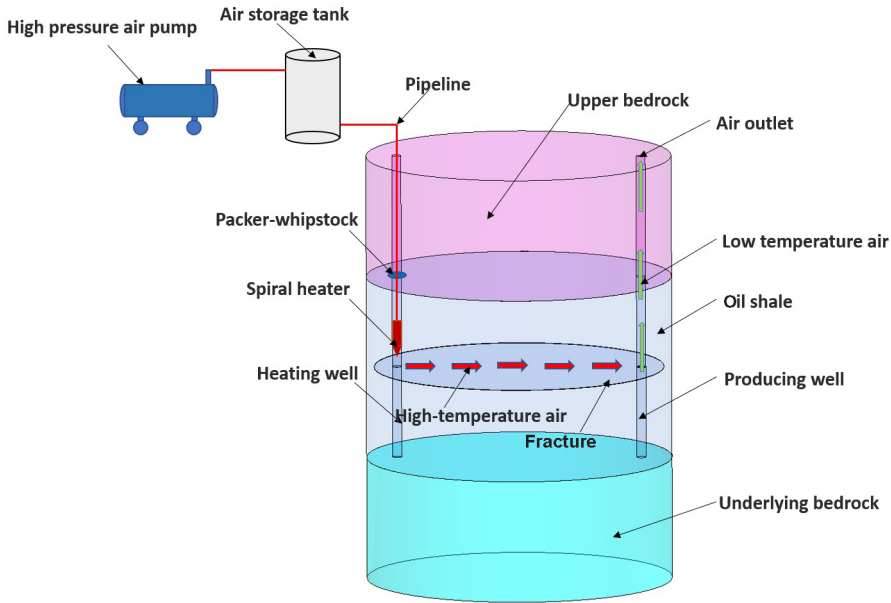


Fig. 1. Schematic diagram of oil shale in-situ heating and cracking.

temperature air generated by heating in the production well permeates into the oil shale area through the fractures generated by fracturing, and oil shale is quickly cracked and produces shale oil and gas under the high-temperature heating in air. After heating, the low-temperature air flows out through the production well, and shale oil and gas are collected at the production well after the heating stops.

3. Modeling and numerical simulation methods

3.1. Heat transfer model of oil shale

In the process of in-situ heating and cracking of oil shale described in this article, air flows through a high-pressure air pump on the ground towards a gas storage tank, which serves as a gas buffer. The air then flows through pipes to a spiral heater located in a heating well. The high-temperature air heated by the spiral heater flows through the fractures towards the production well, transferring energy to the oil shale along the way. Due to the temperature difference between the oil shale surrounding the fractures and the nearby oil shale, heat is transferred to the lower-temperature oil shale through heat conduction.

The governing equations for the temperature field during the in-situ heating and cracking of oil shale are derived from the continuity equation, momentum equation and energy equation [30, 31]:

$$\lambda \nabla^2 T = \rho c + Q(x, y, z). \quad (1)$$

Initial conditions:

$$T(x, y, z, 0) = T_0. \quad (2)$$

Boundary conditions:

$$T|_{\Gamma_1} = T_w(x, y, z, t) \quad \Gamma \in \Gamma_1, \quad (3)$$

$$\lambda \left. \frac{\partial T}{\partial n} \right|_{\Gamma_2} = q(x, y, z, t) \quad \Gamma \in \Gamma_2, \quad (4)$$

$$\lambda \left. \frac{\partial T}{\partial n} \right|_{\Gamma_3} = h(T_2 - T) \quad \Gamma \in \Gamma_3, \quad (5)$$

where T is the temperature of oil shale formation; t is time; λ is the coefficient of heat conduction for oil shale; c is the specific heat conductivity of oil shale; Q is the source sink term; T_0 is the initial temperature of oil shale; T_w is the wall temperature; T_2 is the fluid temperature on the boundary; q is the fluid density on the boundary; h is the heat transfer coefficient of the boundary; Γ means all the boundary conditions of the control body.

The non-steady-state mathematical model of thermal conduction for oil shale in-situ heating and cracking is composed of the above-mentioned control equations for the temperature field in the oil shale region, initial conditions and boundary conditions [29].

3.2. Geometric model establishment

According to the national oil shale data, Jilin Province in China has abundant oil shale resources, ranking first in the country in terms of oil shale reserves. The thickness of oil shale in this region is usually less than 10 m [32]. Figure 2 displays a three-dimensional mathematical model established for this oil shale. The upper and lower bedrocks in Model I have a thickness of 3 m each, the middle oil shale has a thickness of 6 m and a diameter of 10 m. There is a horizontal and uniform crack in the middle of oil shale with a thickness of 10 mm, a diameter of 9.5 m and a distance of 3 m from the upper and lower bedrocks. The heating well and the production well are spaced 8 m apart.

To investigate the effect of the number of cracks on the in-situ heating and cracking of oil shale and find its optimal in-situ mining plan, as shown in Figure 2, Model II and Model III were established based on Model I, with a single crack changing to double and triple cracks, respectively. For Model II,

the upper and lower fractures were 2 m away from the upper and lower base rocks, respectively, and the distance between the upper and lower fractures was 2 m. For Model III, the upper and lower fractures were 1.5 m away from the upper and lower base rocks, respectively, and the distance between the upper and middle fractures and the middle and lower fractures was 1.5 m.

To investigate the effect of crack width on the in-situ heating and cracking of oil shale and find its optimal in-situ mining plan, Model IV and Model V were developed. In Model IV, the crack width is reduced by 20% based on Model I, while in Model V, the crack width is increased by 20% based on Model I. The crack widths in Model IV and Model V are 8 mm and 12 mm, respectively.

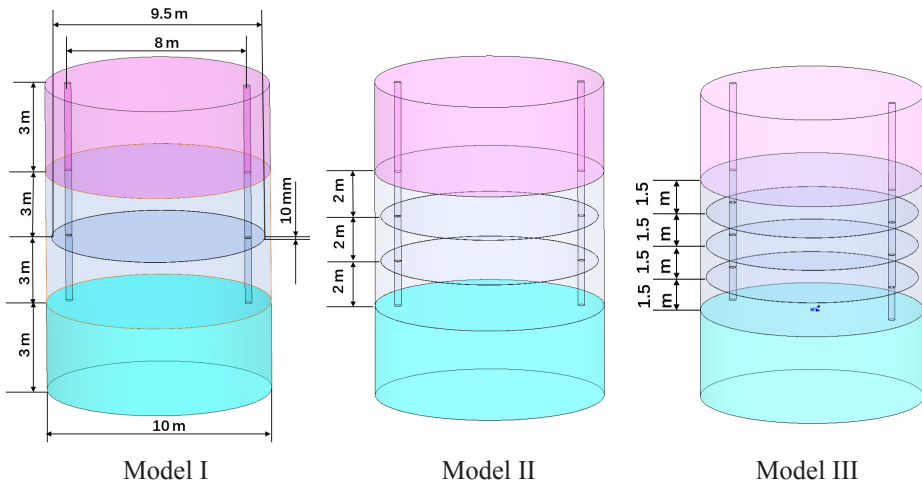


Fig. 2. Oil shale geometric model.

3.3. Simulation calculation and analysis

In this paper, Fluent software was used for numerical simulation to analyze the variation in the oil shale temperature field with crack number, crack width and gas injection rate.

In order to more accurately analyze the oil production capacity of oil shale, this paper adopts the oil shale production rate, which refers to the cumulative oil production rate of oil shale heated to the oil production temperature. The cracking of oil shale mainly occurs at 573.15–723.15 K. The oil shale production rate is defined as follows [33]:

$$\eta_{total} = 0.2\eta_{573.15-623.15} + 0.5\eta_{623.15-673.15} + 0.8\eta_{673.15-723.15} + \eta_{\geq 723.15}, \tag{6}$$

where $\eta_{573.15-623.15}$, $\eta_{623.15-673.15}$, $\eta_{673.15-723.15}$ and $\eta_{\geq 723.15}$ respectively represent the oil shale production rate at temperatures of 573.15–623.15 K, 623.15–673.15 K, 673.15–723.15 K and ≥ 723.15 K.

During the numerical simulation of the temperature field in the in-situ heating and cracking process of oil shale, the model is based on the following basic assumptions:

- 1) The size of the shale fractures remains uniformly unchanged during the entire heating process.
- 2) When the temperature of the entire oil shale formation exceeds 723.15 K, it is assumed that the shale has completely cracked throughout the region.

4. Analysis of influencing factors

4.1. Physical parameters

On investigating the effects of fracture number, fracture width and gas injection rate on the temperature field of the in-situ thermal cracking of oil shale, the initial temperature of the latter is set to 300 K, and that of the upper and lower bedrocks is 300 K, too. High-temperature air at 900 K is injected into the heating well and the rock boundary temperature is set to 300 K. The gas injection port is a mass flow inlet with a mass flow rate given in Table 1, and the gas outlet is a pressure outlet with a pressure of 0.1 MPa. The physical parameters of oil shale, bedrock and air are presented in Table 2 [31].

Table 1. Oil shale models corresponding to the mass flow rates of gas injected into the heating well

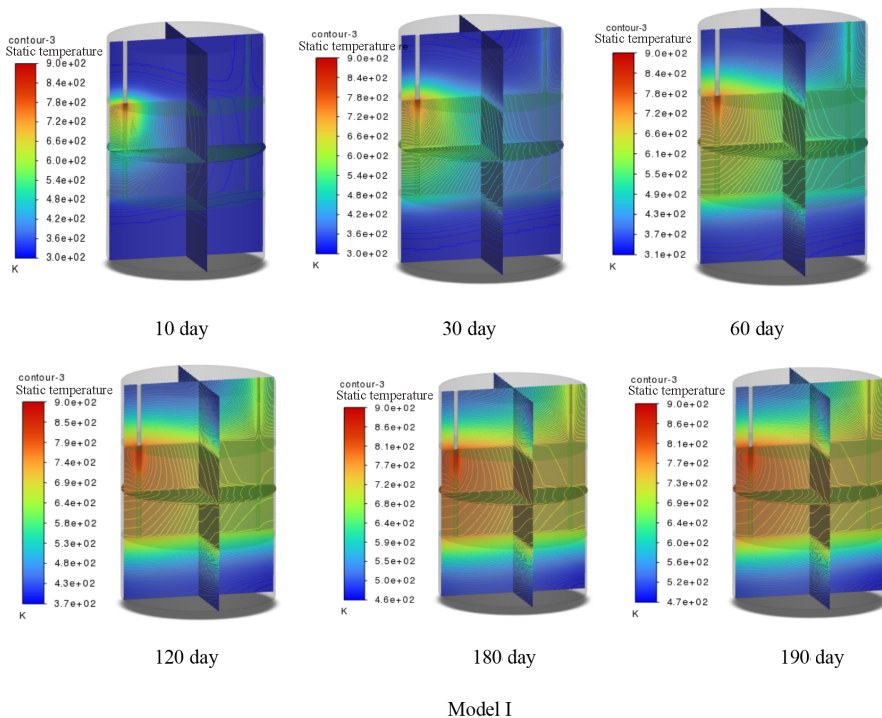
| Parameter | Model I | Model II | Model III |
|----------------------|---------|----------|-----------|
| Mass flow rate, kg/s | 0.3 | 0.4 | 0.5 |

Table 2. Physical parameters of oil shale

| Parameter | Density, $\text{kg}\cdot\text{m}^{-3}$ | Thermal conductivity, $\text{W}\cdot(\text{m}\cdot\text{K})^{-1}$ | Specific heat capacity, $\text{kJ}\cdot(\text{kg}\cdot\text{K})^{-1}$ | Dynamic viscosity, $\text{kg}\cdot(\text{m}\cdot\text{s})^{-1}$ |
|-----------|--|---|---|---|
| Air | 1.225 | 1006.43 | 0.024 | 1.789410^{-5} |
| Bedrock | 2700 | 1.0 | 1200 | – |
| Oil shale | 2500 | 2.5 | 2000 | – |

4.2. Fracture number

Figure 3 demonstrates the distribution cloud map of the oil shale in-situ heating and cracking with crack number over time at a mass flow rate of 0.3 kg/s and a temperature of 900 K. It is revealed that as the in-situ heating time of oil shale increases, the temperature of the oil shale region continues to rise. Model I, Model II and Model III reached 723.15 K in the oil shale region at 190, 140 and 200 days, respectively, indicating a complete cracking of this region. During the rapid heating phase of oil shale in-situ heating and cracking, the cracking mainly occurred near the heating well and the temperature difference between the oil shale region and the high-temperature air was large, resulting in a rapid heat transfer and fast temperature rise of the oil shale region. During the slow heating phase of oil shale in-situ heating and cracking, the temperature difference between the oil shale region and the high-temperature air was relatively small, resulting in a slow temperature rise of this region. However, due to the accumulation of a large amount of heat during the rapid heating phase, an extensive cracking occurred in the oil shale region with continuous heating during this phase, making it the fastest stage of cracking. During the constant temperature phase of oil shale in-situ heating and cracking, at the end of the heating process as the heating time increased, the temperature of the oil shale region remained constant. This is mainly because the oil shale region reached a relatively steady state at this stage, and the high-temperature air flowed out of the production well mainly along the cracks where the temperature was the same as that of the surrounding oil shale.



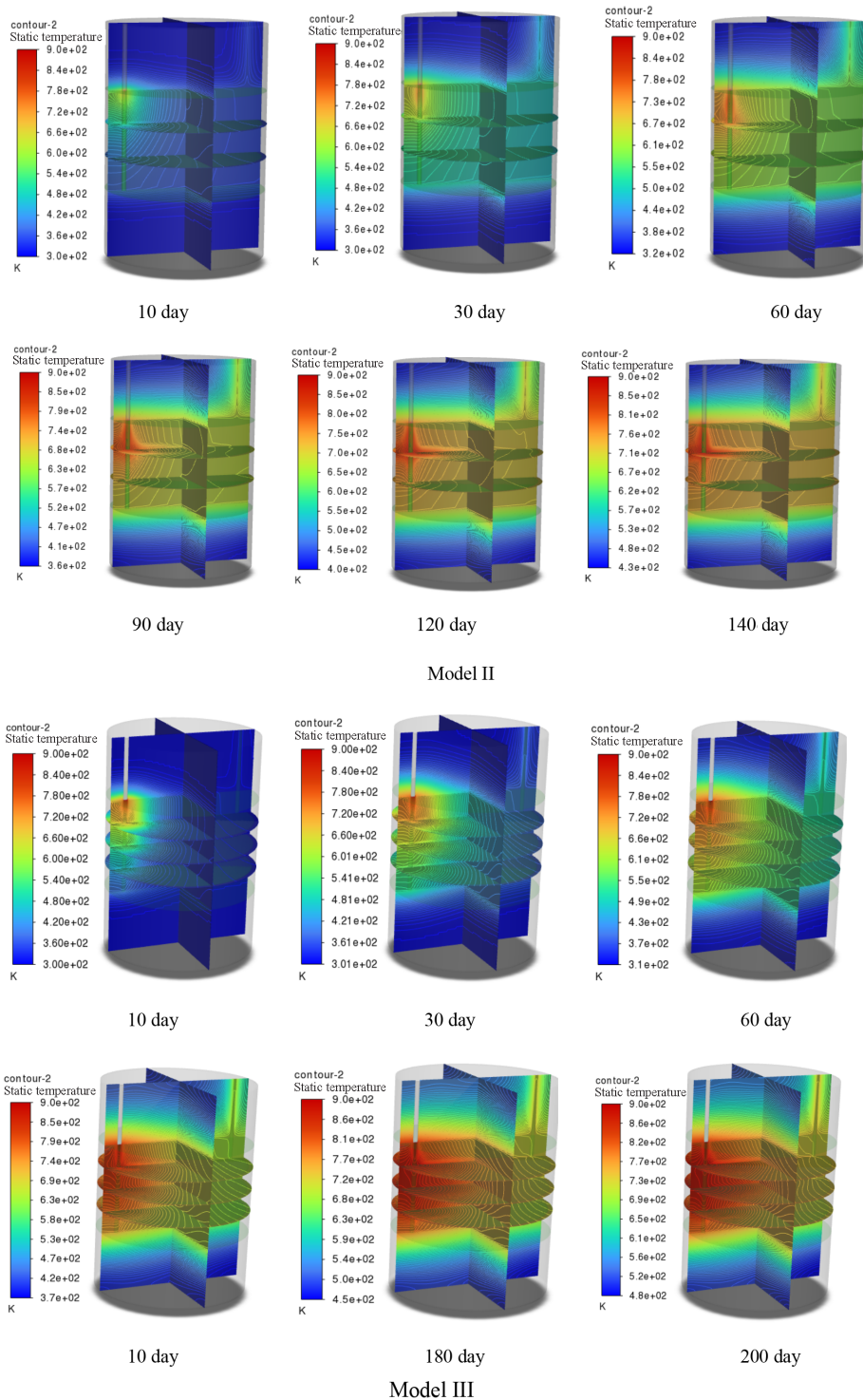


Fig. 3. Temperature distribution contour maps of oil shale in-situ heating and cracking with fracture number over time.

Figure 4 exhibits the speed distribution cloud map of the oil shale in-situ heating and cracking process with fissure number. It can be observed that during this process, gas flows into the production well and primarily heats the oil shale area through the fissures, flowing eventually out of the production well. At this, the speed of Model I with a single fissure is the highest, followed by that of Model II with two fissures, while the speed of Model III with three fissures is the lowest. At the same time, the maximum speed during the in-situ heating and cracking process of oil shale occurs at the intersection between the heating well and the fissure and at the intersection between the production well and the fissure. This is mainly because the cross-section undergoes a sudden change and the thickness of the fissure is relatively thin.

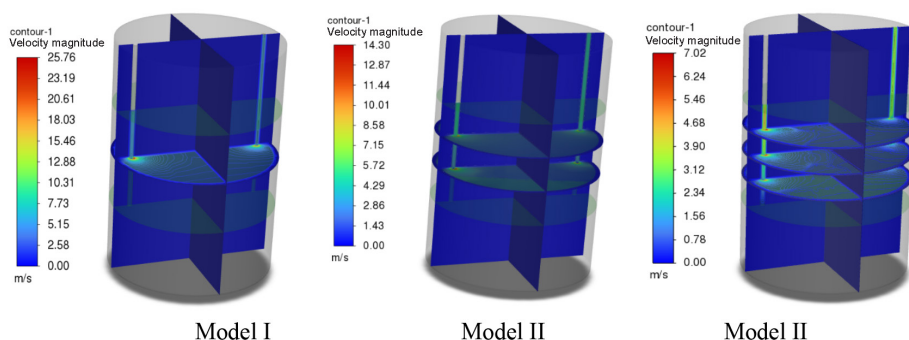


Fig. 4. Speed distribution cloud maps of the oil shale in-situ heating and cracking process with fissure number.

Figure 5a displays the variation in cumulative oil production rate with heating time during the in-situ heating and cracking process of oil shale. From the figure it can be seen that in the said process, the heating rate of Model II is the highest and the oil shale area is completely cracked after 140 days. The heating rate of Model I is the second highest and the oil shale area reaches 100% cracking after 190 days, while that of Model III is the lowest and the cracking of the entire oil shale area is completed after 200 days. The in-situ heating and cracking of oil shale in the three models mainly occurs in the first 130 days, during which the oil production rates of Models I, II and III are 78.35%, 95.91% and 78.51%, respectively. The heating rate of Model II with dual fissures is 26.32% higher than that of Model I with a single fissure, while the heating rate of Model III with triple fissures is 5.26% lower than that of Model I with a single fissure. The main reason for this is that with increasing number of fissures, the gas flow rate in each fissure layer decreases and that of the fissures near the lower part of oil shale is relatively low. In the later stage of heating, the oil shale near the bottom right area of the production well heats up slowly. Therefore, the in-situ heating and cracking time of oil shale

is prolonged. The results indicate that among the three models with different numbers of fissures, the heating effect of Model II with dual fissures is the highest.

In Figure 5b, the variation in 10-day cumulative oil production rate during the in-situ heating and cracking process of oil shale with heating time is shown. From the figure it can be seen that the early 10-day oil production rate is low, which is mainly due to the large temperature difference between oil

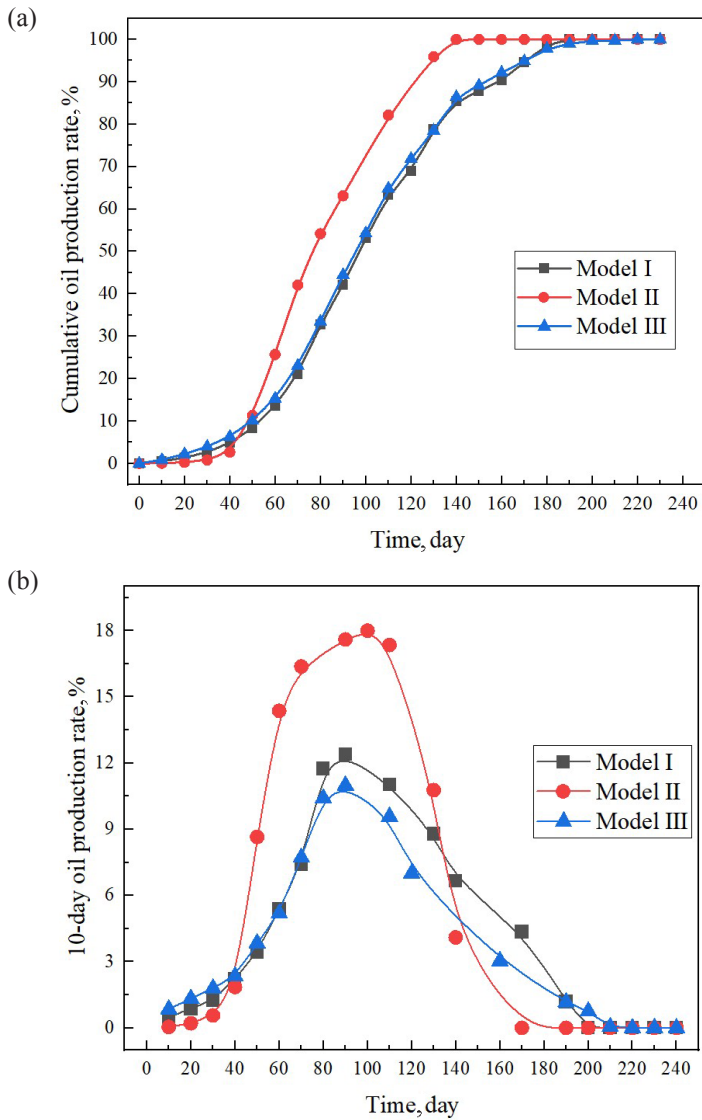


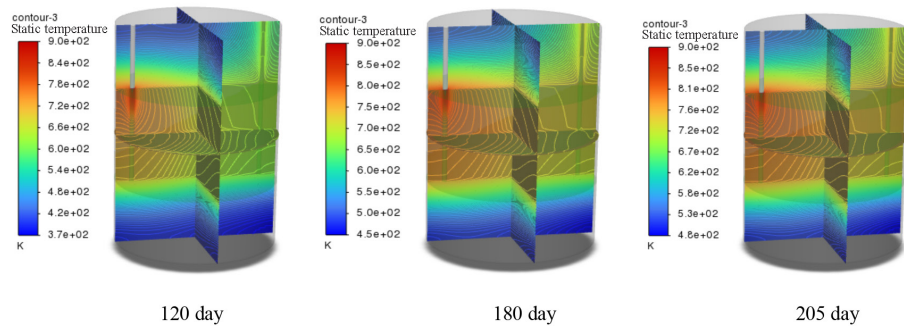
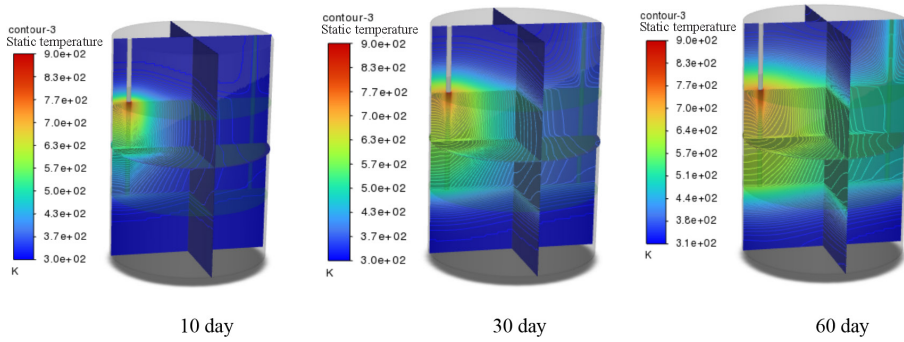
Fig. 5. Graphs of the variation in cumulative oil production rate (a) and 10-day oil production rate of shale oil (b) with time during oil shale in-situ heating and cracking.

shale and the high-temperature air in the early stage. The high-temperature air and oil shale rapidly exchange heat, while the temperature of the latter near the heating well rises rapidly. At this, the region of the entire oil shale area that can reach the cracking temperature mainly spreads around the heating well, which results in a low early 10-day oil production rate. The mid-term 10-day oil production rate is relatively high. At a heating time of 110 days, the oil production rates of Models I, II and III are the highest, being respectively 11.02%, 17.99% and 9.58%. At this stage, under the continuous accumulation of heat in the early stage, the temperature of the oil shale area has become relatively high. With the continuous heating in this stage, the cracking rate of oil shale has significantly increased, while the stage represents also the main period of oil shale cracking. In the later stage, due to the concentration of noncracked oil shale mostly around the production well and far from the heating well, the heating process significantly expands the heat to the basement area, resulting in a significant decrease in heating efficiency. This stage is also a period of slow cracking of oil shale.

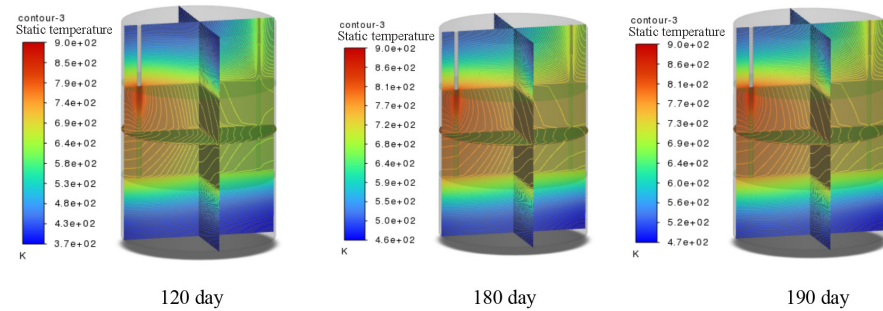
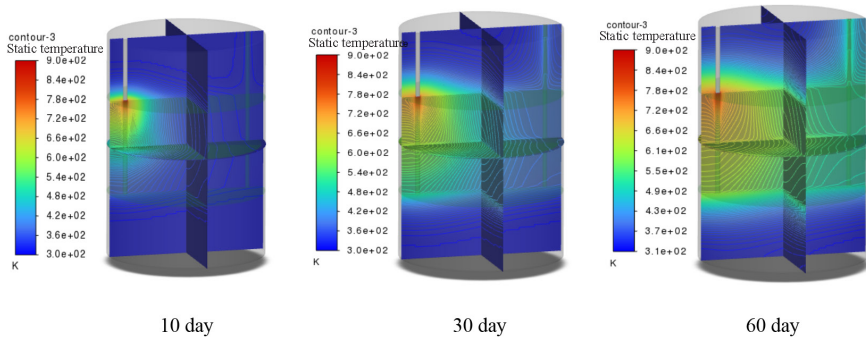
4.3. Fracture width

Figure 6 presents the temperature distribution cloud maps of the oil shale in-situ heating and cracking process with crack width over time. Based on Model I, Models IV and V were established by reducing and increasing the crack width by 20%, respectively. High-temperature gas with a mass flow rate of 0.3 kg/s and a temperature of 900 K was injected into Models IV, I and V. In the early stage of oil shale in-situ heating and cracking, due to the presence of cracks in the oil shale region, the heat transfer rate in the vicinity of the crack was significantly higher than that in the surrounding area. With increasing heating time of the oil shale region, it was found that appropriately increasing the crack width accelerated the in-situ heating and cracking of oil shale. Models IV, I and V completely cracked the oil shale region in 205, 190 and 180 days, respectively.

Figure 7a shows the variation in cumulative oil production rate with time during the in-situ heating and cracking of oil shale. As can be seen from the figure, with increasing in-situ heating and cracking time of oil shale, the oil production rate of Model V is the highest, followed by that of Model I, while the one of Model IV is the lowest. When the oil shale region is completely cracked, Model IV is 15 days slower than Model I, with a heating rate reduction of 7.89%, and Model V is 10 days faster than Model I, with a heating rate increase of 5.26%. In the first 40 days, the in-situ heating and cracking of oil shale is relatively slow, mainly due to its low initial temperature when the high-temperature gas rapidly exchanges heat with the oil shale region and the oil shale temperature rises most quickly during this stage. From 40 to 160 days, the heat is accumulated in the early stage of heating, resulting in a higher temperature in the oil shale region. With continuous heating, the cracking rate



Model IV



Model I

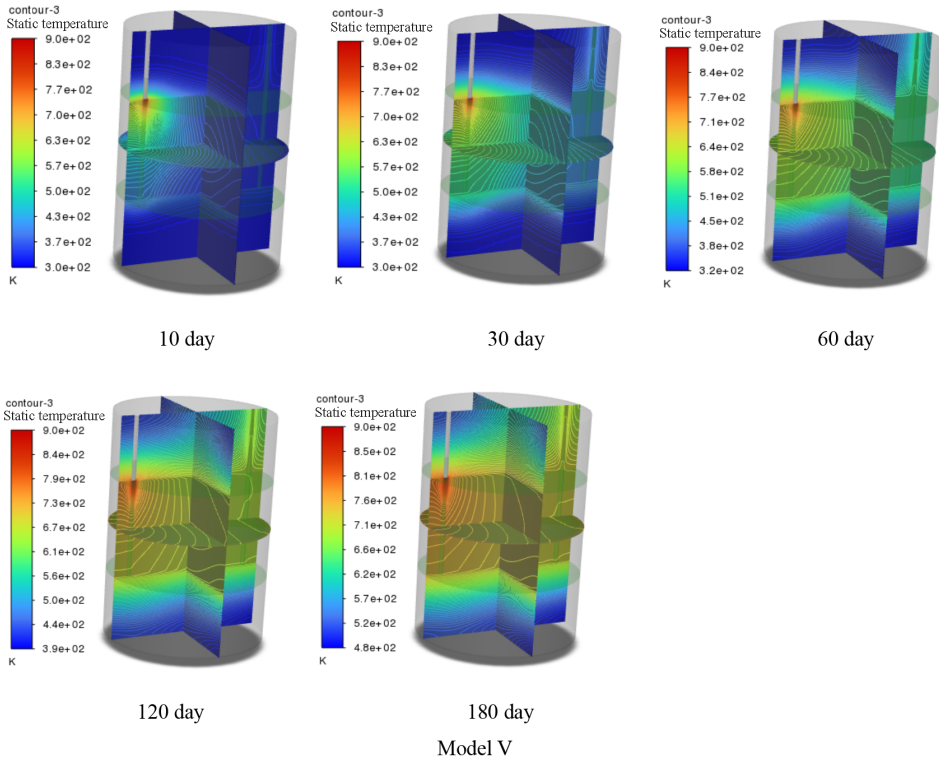


Fig. 6. Temperature distribution cloud maps of the oil shale in-situ heating and cracking process with heating time and crack width.

of oil shale increases significantly during this stage and the cracking takes place during the entire heating process, mostly. After 160 days, the in-situ heating and cracking rate of oil shale begins to decline and a large amount of heat flows to the bedrock, reducing the heating efficiency. Therefore, appropriately increasing the crack width is beneficial for improving the in-situ heating and cracking rate of oil shale.

As shown in Figure 7b, the average temperature rise rate of oil shale during the in-situ heating and cracking process varies with time. The figure reveals that for all three models, the average temperature rise rate of oil shale decreases as the heating time increases. In the first two months, Model V exhibited the highest temperature rise rate, averaging 174.03 K/m and 95.86 K/m, respectively. In the next four months, as the temperature difference between the oil shale region and the high-temperature gas decreases and the heat transfer rate slows down, the temperature rise rate of oil shale decelerates and the curvature of the average temperature rise rate curve gradually becomes horizontal. The average temperature rise rates of Model V are 61.78 K/m, 44.73 K/m, 34.52 K/m and 27.68 K/m. The temperature rise rate of Model I in the first two months is the second highest, being respectively 146.45 K/m and

102.51 K/m. The temperature rise rate of Model IV in the first two months is the lowest, 132.99 K/m and 94.48 K/m, respectively. Because the temperature rise rate of Model IV is low in the early stage and the temperature of the oil shale layer is relatively low, the temperature difference between the oil shale region and the high-temperature gas is relatively large, resulting in the highest temperature rise rate of Model I in the next four months, with averages of 70.67 K/m, 53.74 K/m, 41.34 K/m and 32.73 K/m.

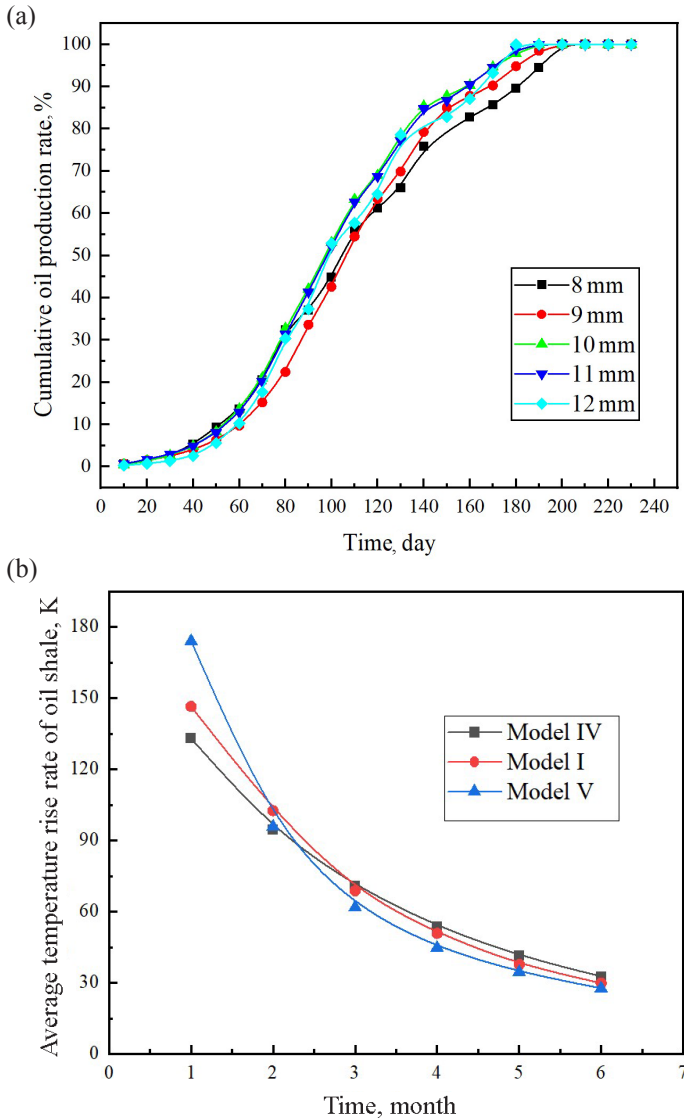
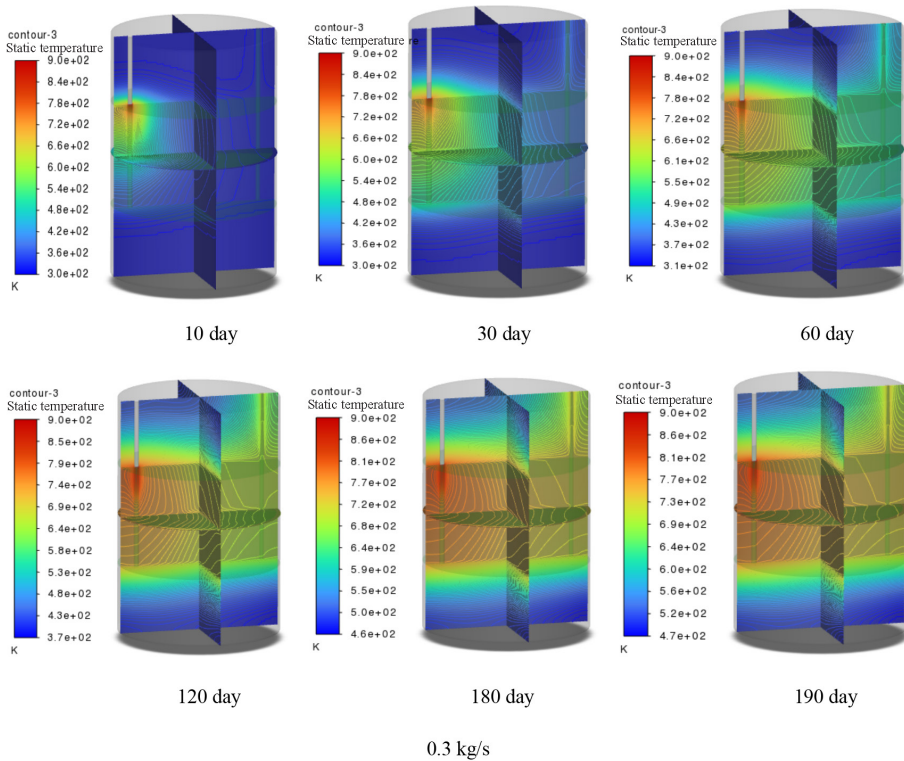


Fig. 7. Graphs of the variation in cumulative oil production rate and average heating rate of shale oil during the oil shale in-situ heating and cracking process with fracture width over time: (a) cumulative oil production rate; (b) average temperature rise rate of oil shale.

4.4. Injection rate

Figure 8 presents the temperature field distribution cloud maps of the oil shale in-situ heating and cracking with gas injection flow rate. The 900 K high-temperature gas with a mass flow rate of 0.3 kg/s, 0.4 kg/s and 0.5 kg/s was respectively introduced into Model I. With the increase of heating time, the temperature field diffusion range and the oil shale cracking area continuously expand. The high-temperature air continually heats the oil shale along the fractures and the temperature field of the oil shale area diffuses forward in a ripple shape. When the heating time reaches 110 days, the 0.5 kg/s high-temperature air will first completely crack the oil shale in this area. When the heating time reaches 140 days, the 0.4 kg/s high-temperature air will completely crack the oil shale in the given area. When the heating time reaches 190 days, the 0.3 kg/s high-temperature air will completely crack the oil shale in the area concerned. With the mass flow rate increased from 0.3 kg/s to 0.4 kg/s, the in-situ heating and cracking time of oil shale is shortened by 26.32%. When the mass flow rate is increased from 0.3 kg/s to 0.5 kg/s, the in-situ heating and cracking time of oil shale is reduced by 42.11%.



0.3 kg/s

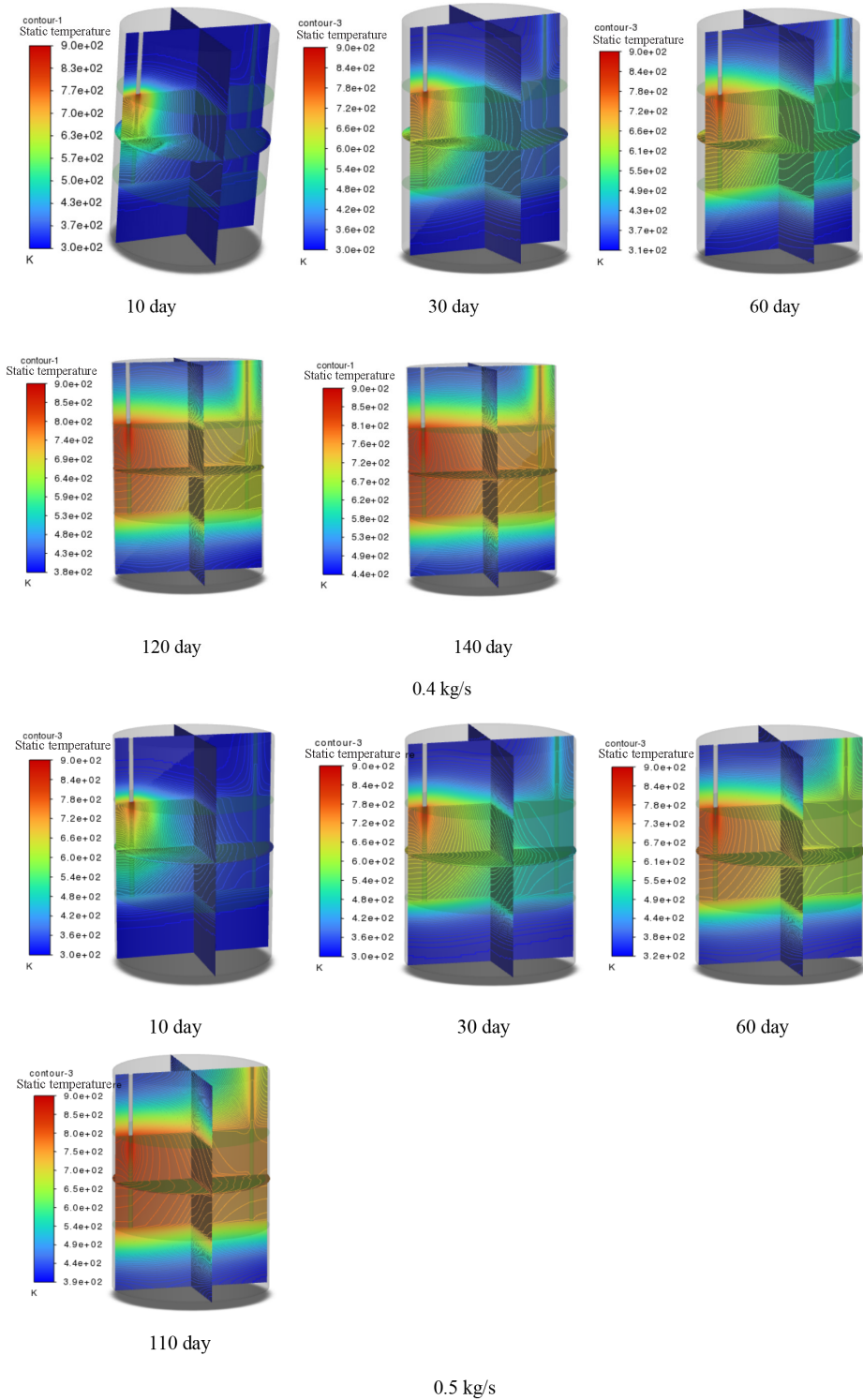
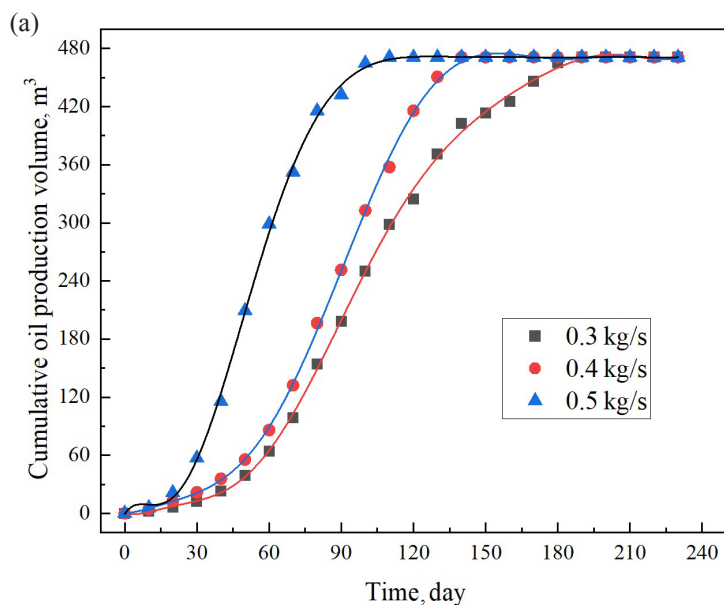


Fig. 8. Temperature field distribution contour map of oil shale in-situ heating and cracking with injection gas flow rate as a function of heating time.

The graph in Figure 9 shows the variation in the cumulative oil production volume and the 10-day oil production volume of oil shale during in-situ heating and cracking. According to Figure 9a, as the injection gas flow rate increases, the in-situ heating and cracking of oil shale happen more rapidly. With the increase of heating time, the high-temperature gas with a mass flow rate of 0.5 kg/s is the first to complete the cracking at 110 days, with a cumulative oil production volume of 471 m³. The in-situ heating and cracking with high-temperature gas with a mass flow rate of 0.4 kg/s lags behind that with high-temperature air with a mass flow rate of 0.5 kg/s by 30 days. The in-situ heating and cracking speed with high-temperature air with a mass flow rate of 0.3 kg/s is relatively low. In the early stage of heating, the in-situ heating and cracking of oil shale takes place relatively slowly because its temperature is low at the beginning and the high-temperature gas exchanges heat with oil shale rapidly. During this stage, the temperature of oil shale increases most significantly. In the middle stage of heating, the in-situ heating and cracking of oil shale occurs at the highest speed. In the later stage of heating, because the temperature difference between the oil shale region and the high-temperature air is small, the heat transfer between the high-temperature gas and the oil shale slows down, leading to a decrease in the cracking speed of oil shale.

Figure 9b shows that the higher the mass flow rate, the larger the 10-day oil production volume and the higher the peak value of oil production volume. In the early stage, the 10-day oil production volume is relatively small, and the high-temperature air with mass flow rates of 0.5 kg/s, 0.4 kg/s and 0.3 kg/s reaches the peak value of 10-day oil production volume at 50th, 90th and 100th days, respectively, with volumes of 93.68 m³, 67.26 m³ and 51.92 m³. Afterward, the oil shale in-situ heating and cracking start to decrease the oil production volume, and they are completely cracked at 110th, 140th and 190th days, respectively.



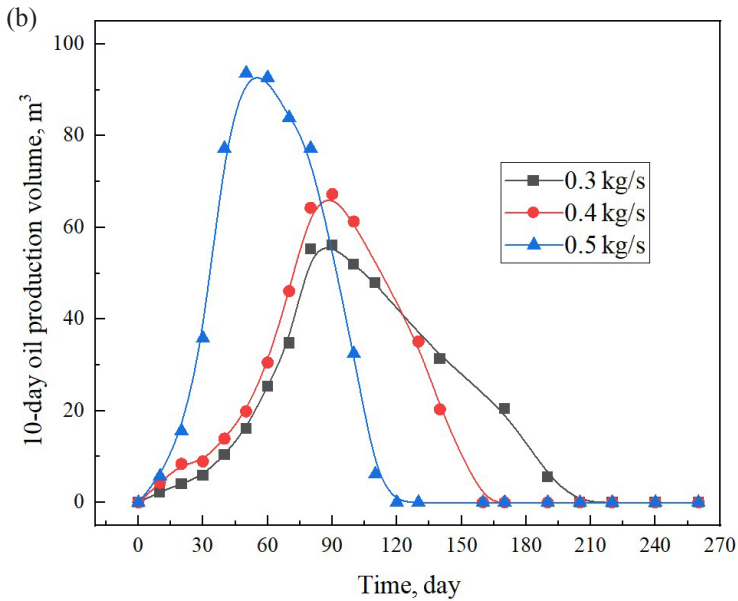


Fig. 9. Graphs of the variation over time in cumulative oil production volume (a) and 10-day oil production volume of shale oil (b) during the oil shale in-situ heating and cracking process.

5. Conclusions

1. During the in-situ heating and cracking process of shale oil, when there are two fractures in the shale region of Model II, the heating rate of shale is the highest, being 26.32% higher than that of Model I. The peak of the 10-day oil production rate is the highest, those of Models I, II and III all appearing at around 90 days. The results indicate that increasing the number of fractures appropriately is beneficial to improving the heating rate of shale.
2. During the in-situ heating and cracking process of oil shale, Model I completes the entire shale cracking in the shale area at 190 days, Model IV is 15 days slower than Model I with a 7.89% decrease in heating rate, and Model V is 10 days faster than Model I with a 5.26% increase in heating rate. The results indicate that appropriately increasing the width of shale fractures in the shale area can increase the heating rate of oil shale in the early stage and also contribute to the rise of the in-situ heating and cracking rate.
3. During the in-situ heating and cracking process of oil shale, when the mass flow rates of high-temperature air were 0.5 kg/s, 0.4 kg/s, and 0.3 kg/s, respectively, the oil shale region was completely cracked on the 110th,

140th and 190th days, and the peak value of the 10-day oil production volume was reached on the 50th, 90th and 100th days, respectively. The volumes of the cracked shale regions were 93.68 m³, 67.26 m³ and 51.92 m³, respectively. The heating rates of high-temperature air with mass flow rates of 0.5 kg/s and 0.4 kg/s were increased by 42.11% and 26.32%, respectively, compared to Model I. The results showed that as the gas flow rate increased, the temperature of the oil shale region increased faster, reaching the peak production rate of oil in a shorter time, and the peak value was also larger, indicating that the cracking of the oil shale region took place more rapidly.

Acknowledgments

Tengfei Sun and Hao Liu as the first two co-authors of the article are acknowledged for their equal contribution to this work. The authors gratefully acknowledge the financial support of the National Nature Science Foundation of China (No. 52074018, No. 52274001) and the financial support of Fundamental Research Funds for the Central Universities (buctrc202017).

The publication costs of this article were partially covered by the Estonian Academy of Sciences.

REFERENCES

1. Ma, J. X., Xue, L. F., Zhao, J. M., Bai, F. T. Numerical simulation and design optimization of temperature field of oil shale in situ pyrolysis and exploitation. *Science Technology and Engineering*, 2019, **19**(5), 94–103 (in Chinese).
2. Zhang, M., Guo, W., Li, Q., Sun, Z., Wang, Z., Zhao, S., Qu, L. Research on heat transfer characteristics and numerical simulation of oil shale in-situ pyrolysis heater with spiral baffle. *Exploration Engineering (Rock & Soil Drilling and Tunneling)*, 2018, **45**(7), 62–65 (in Chinese).
3. Li, N. Y., Wang, Y., Chen, F., Han, Y. L., Chen, W. B., Kang, J. Development status and prospects of in-situ conversion technology in oil shale. *Special Oil & Gas Reservoirs*, 2022, **29**(3), 1–8 (in Chinese).
4. Wang, Z. D. *Study on Heat Transfer Performance and Heating Efficiency of Electric Heater with Continuous Helical Baffles for Oil Shale in-Situ Conversion*. PhD Thesis, Jilin University, 2021.
5. Li, X. X. *Numerical Simulation of Temperature Field in Situ Modified by Electric Heating of Oil Shale*. MS Thesis, Northeastern Petroleum University, 2021 (in Chinese).
6. Fu, C., Ding, H., Chen, W. M. Resources distribution and comprehensive utilization of oil shale and coal symbiosis in China. *Coal Quality Technology*, 2021, **36**(3), 1–13.

7. Zhu, Y. *Study on the Influence of Oil Shale Bedding Planes on Its Mechanical Properties, Fracture Initiation and Extension*. PhD Thesis, Jilin University, 2022 (in Chinese).
8. Jiang, P. F. *Experimental Research on Oil Shale In-Situ Conversion by Acid Fracturing-Heat Injection*. PhD Thesis, Jilin University, 2016 (in Chinese).
9. Kang, Z., Zhao, Y., Yang, D. Review of oil shale in-situ conversion technology. *Appl. Energy.*, 2020, **269**, 115121.
10. Pan, Y., Mu, J., Ning, J., Yang, S. Research on in-situ oil shale mining technology. *Int. J. Pharm. Sci. Inven.*, 2012, **1**(1), 1–7.
11. Chen, C., Wang, W., Sun, Y., Guo, W., Yan, X., Wang, H., Zhao, G., Wen, J., Fang, Q., Liu, X. Influence of the heat transfer efficiency of oil shale in situ fragmentation. In: *Progress of Geo-Disaster Mitigation Technology in Asia* (Wang, F., Miyajima, M., Li, T., Shan, W., Fathani, T. F., eds.), 2013, 577–583.
12. Zhao, F., Xi, C., Zhang, X., Shi, X., Yang, F., Mu, H., Guan, W., Jiang, Y., Wang, H., Babadagli, T., Li, H. Evaluation of a field-wide post-steam in-situ combustion performance in a heavy oil reservoir in China. In: *SPE Russian Petroleum Technology Conference*. OnePetro, 26–29 October 2020, Paper Number SPE-201815-MS.
13. Song, X., Zhang, C., Shi, Y., Li, G. Production performance of oil shale in-situ conversion with multilateral wells. *Energy*, 2019, **189**, 116145.
14. Gao, Y., Long, Q., Su, J., He, J., Guo, P. Approaches to improving the porosity and permeability of Maoming oil shale, South China. *Oil Shale*, 2016, **33**(3), 216–227. <https://doi.org/10.3176/oil.2016.3.02>
15. Wang, L., Yang, D., Li, X., Zhao, J., Wang, G., Zhao, Y. Macro and meso characteristics of in-situ oil shale pyrolysis using superheated steam. *Energies*, 2018, **11**(9), 2297.
16. Hu, S., Wu, H., Liang, X., Xiao, C., Zhao, Q., Cao, Y., Han, X. A preliminary study on the eco-environmental geological issue of in-situ oil shale mining by a physical model. *Chemosphere*, 2022, **287**, 131987.
17. Wang, G., Liu, S., Yang, D., Fu, M. Numerical study on the in-situ pyrolysis process of steeply dipping oil shale deposits by injecting superheated water steam: A case study on Jimsar oil shale in Xinjiang, China. *Energy*, 2022, **239**, Part C, 122182.
18. He, W., Sun, Y., Shan, X. Organic matter evolution in pyrolysis experiments of oil shale under high pressure: Guidance for in situ conversion of oil shale in the Songliao Basin. *J. Anal. Appl. Pyrolysis*, 2021, **155**, 105091.
19. Wang, Z., Yang, F., Fu, D., Ma, L., Duan, Z., Wang, Q., Kang, S., Guo, W. Economic and heating efficiency analysis of double-shell downhole electric heater for tar-rich coal in-situ conversion. *Case Stud. Therm. Eng.*, 2023, **41**, 102596.
20. Kang, Z. Q., Zhao, Y. S., Yang, D. Physical principle and numerical analysis of oil shale development using in-situ conversion process technology. *Acta Petrolei Sinica*, 2008, **29**(4), 592–595+600 (in Chinese).

21. Yang, H., Duan, Y. X. A feasibility study on in-situ heating of oil shale with injection fluid in China. *J. Petrol. Sci. Eng.*, 2014, **122**, 304–317.
22. Jiang, P., Zhang, D., Li, B., Son, C. Design and numerical simulation of in-situ pyrolysis of oil shale through horizontal well fracturing with nitrogen injection. *Int. J. Heat Technol.*, 2021, **39**(2), 417–423.
23. Li, Y. B., Xue, L. F., Ma, J. X. Numerical simulation of the changes of porosity and permeability in in-situ pyrolysis of oil shale. *Science Technology and Engineering*, 2018, **18**(34), 43–50 (in Chinese).
24. Xue, J. X., Liu, Z. H. Numerical simulation of the temperature field distribution of oil shale under in-situ process by the electricity heating method. *Chinese Journal of Underground Space and Engineering*, 2015, **11**(3), 669–672 (in Chinese).
25. Jiang, P. F., Sun, Y. H., Guo, W., Li, Q. Heating technology and heat transfer simulation for oil shale of in-situ pyrolysis by fracturing and nitrogen injection. *Journal of Northeastern University (Natural Science)*, 2015, **36**(9), 1353–1357+1368 (in Chinese).
26. Wang, Y. Y., Xue, L. F., Sun, X. Impact of fracture occurrence and relative position on the heating effect in oil shale in-situ mining. *Science Technology and Engineering*, 2019, **19**(35), 141–147 (in Chinese).
27. Zheng, Y., Lei, G., Yao, C., Fu, J., Wang, L., Zhang, X., Jia, X. A calculation model about reservoir thermal efficiency of in-situ upgrading for oil shale via steam injection. *J. Petrol. Sci. Eng.*, 2020, **192**, 107267.
28. Wang, B. Q. *Numerical Simulation of Gas Injection In-Situ Exploit of Oil Shale and Underground Frozen Wall Formation*. MS Thesis, Jilin University, 2014 (in Chinese).
29. Zhou, K. *Numerical Simulation of Temperature Field and Field Test of In-Situ Pyrolysis of Oil Shale with Hot Nitrogen*. MS Thesis, Jilin University, 2017 (in Chinese).
30. Jiang, Y. D., Yang, X. Y., Xian, X. F., Xiong, L., Yi, J. The infiltration equation of coal bed under the cooperation of stress field, temperature field and sound field. *Journal of China Coal Society*, 2010, **35**(3), 434–438 (in Chinese).
31. Sun, C. L., Wang, Y., Shao, H. L., An, J. N., Zhao, Y. D., Yang, Q. R. Numerical simulation of the development of oil shale in situ electrical temperature field. *Journal of Liaoning Shihua University of Petroleum & Chemical Technology*, 2015, **35**(4), 40–43 (in Chinese).
32. Shi, W. P., Zheng, H., Wang, B. Q. Numerical simulation of electric heating for oil shale in horizontal wells. *Oil Drilling & Production Technology*, 2014, **36**(5), 80–83 (in Chinese).
33. Zhao, J. M., Cao, D. F., Liu, Y. M., Xing, S. F. Fluid-thermal-solid coupling simulation of oil shale in-situ pyrolysis by horizontal well pattern. *Science Technology and Industry*, 2022, **22**(1), 329–337 (in Chinese).